atoms

MDPI

Article

Study of the Hyperfine Structure of Sr II, Ba I and Ba II: An MCDHF Approach for Modeling the Low-Lying Levels

Lorenzo Nezosi [1], Lucas Maison [1], Patrick Palmeri [1,*], Per Jönsson [2] and Michel Godefroid [3]

[1] Physique Atomique et Astrophysique, Université de Mons—UMONS, B-7000 Mons, Belgium; lorenzo.nezosi@student.umons.ac.be (L.N.); lucas.maison@umons.ac.be (L.M.)
[2] Materials Science and Applied Mathematics, Malmö University, SE-205 06 Malmö, Sweden; per.jonsson@mau.se
[3] Spectroscopy, Quantum Chemistry and Atmospheric Remote Sensing, Université Libre de Bruxelles, B-1050 Brussels, Belgium; michel.godefroid@ulb.be
* Correspondence: patrick.palmeri@umons.ac.be

Abstract

Using the Multiconfiguration Dirac–Hartree–Fock method as implemented in the General Relativistic Atomic Structure Package, the magnetic dipole and electric quadrupole hyperfine structure constants were determined for the ground and first excited levels of ^{135,137}Ba II isotopes, as well as for ^{137}Ba I and ^{87}Sr II, to assess the robustness of the developed model. This study builds upon and extends previous investigations by examining the levels involved in resonance lines, with the aim of resolving persistent discrepancies in the hyperfine structure of ^{137}Ba II and ^{87}Sr II. New code developments such as the use of natural orbitals, as well as the addition of polarization effects and Configuration State Function Generators, as implemented in GRASPG, were tested for these heavy elements. The developed strategy allowed us to achieve encouraging results that satisfactorily agree with experiments for all studied levels but $^2D_{5/2}$ in the ^{137}Ba II isotope. This disagreement was also observed in ^{135}Ba II isotope as well as in ^{87}Sr II. With two valence electrons, ^{137}Ba I is definitely more complex, requiring a multireference approach. Even with the latter, the theory–observation disagreement observed for the hyperfine structure of the low-lying levels remains large in comparison with the alkali-like systems. Possible ongoing developments to remediate this issue are discussed in the conclusions.

Keywords: atomic structure; hyperfine structure; MCDHF method; GRASP package; barium; strontium

Academic Editor: Yew Kam Ho

Received: 19 January 2026
Revised: 2 March 2026
Accepted: 3 March 2026
Published: 5 March 2026

1. Introduction

Heavy elements are created in neutron-capture processes. The two most known processes are the s- and r-process. The first one produces half of the elements heavier than iron [1]. It is slow in the sense that neutron density is low enough (10^7–10^{13} neutrons per cm^3) to allow β^- decay of nuclei. It produces elements ranging from Fe to Sr-Y and up to Pb, with lead being the heaviest element generated by this process. The latter r-process, taking place in astrophysical sites where the neutron density is more important ($>10^{20}$ neutrons per cm^3 [2]), does not allow β^- decay between two neutron captures. Only when the neutron flux is exhausted, the unstable nuclei return to stability through a cascade of β^- decay, leading to the formation of elements heavier than Pb. Ranging just in between these two processes, an intermediate process, the i-process, with a neutron

density of 10^{12}–10^{15} neutrons per cm^3 [2] was highlighted by Cowan and Rose [3] in order to explain the observed anomalies in abundances of Sr, Ba, La, and Eu.

In the solar system, the majority of heavy elements are produced in a mix of s- and r-processes. For instance, 82% of Ba is produced by the s-process, but only 6% for Eu. The other part is produced by the r-process [4]. Consequently, Ba is frequently employed as a signature element for the s-process, while Eu serves as one for the r-process. The study of the spectral lines of these elements, as well as their abundance ratio [Ba/Eu], can be used to determine which process dominates the production. For low-metallicity subgiant stars like HD 140283, which is one of oldest stars of the Universe and mainly composed of hydrogen and helium, the r-process elements should be dominant [5]. During nucleosynthesis processes, different Ba isotopes are created: the odd ones are affected by the hyperfine splitting of the energy levels that can be easily resolved by spectrometers. Therefore, they be used to determine abundances of these isotopes via the isotopic ratio $f_{\text{odd, Ba}}$ defined by

$$f_{\text{odd, Ba}} = \frac{\text{N}(^{135}\text{Ba}) + \text{N}(^{137}\text{Ba})}{\text{N(Ba)}}, \quad (1)$$

with N(Ba) being the number of all Ba atoms. The isotopic ratio is key in several studies on the determination of dominant nucleosynthesis processes. Depending on the value of this ratio, Arlandini et al. [4] concluded that a value of $f_{\text{odd,Ba}} \approx 0.46$ was the signature of a Ba r-process creation, while a value of $f_{\text{odd,Ba}} \approx 0.11$ was the marker of the s-process. Whenever the value of $f_{\text{odd,Ba}}$ is located between these two margins, it could mean that a mix of these two processes has occurred. Regarding the HD 140283 star, the uncertainties obtained by Lambert & Allende Prieto [6] were too high to determine the formation process. A more recent study using 3D-LTE spectral line modeling [7] showed that Ba was produced using the r-process, matching the theoretical predictions with $f_{\text{odd,Ba}} \approx 0.38$.

Alternatively, neutral Ba (Ba I) can be used to determine the stellar abundances and therefore the isotopic ratio. Reddy & Lambert [8] showed that the 5535 Å line is unfortunately blended with a Fe I transition for the HD 17925 star, leading to an overestimation of abundances. However, the study of Ba I and very precise atomic data are still needed for the abundance analysis of cool stars [8].

Strontium (Sr) is the second neutron-capture element that shows very strong absorption lines even in metal-poor stars [9]. The Sr II lines are less affected by NLTE effects compared to Ba II, making Sr II a more reliable abundance indicator in some cases [9]. Sr exhibits an electronic structure analogous to that of Ba, but with a lower atomic mass. This makes Sr a valuable system for extended calculations to better analyze potential trends among elements in the same group of the periodic table.

Other types of stars, like Carbon-Enriched Metal-Poor (CEMP) stars, show particular abundance ratios. The CEMP-rs stars, highlighted by Barbuy et al. [10], are interesting because they exhibit overabundances in both s- and r-process elements. Using the Ba II line profiles, studies [11] show that stars like HE 2208–1239 could have heavy elements produced by the i-process. This conclusion still needs to be handled with care as the [Ba/Fe] abundances were taken strictly equal to [Ce/Fe] ones in order to deal with Ba overabundances obtained by considering subordinate excited levels.

Therefore, accurate determination of hyperfine structure (HFS) constants is essential for reliable barium (Ba) abundance analyses, particularly when estimating the odd-isotope fraction $f_{\text{odd,Ba}}$. The Ba II resonance lines, especially at 4554 Å and 4934 Å, are significantly split by HFS due to the presence of odd isotopes (^{135}Ba and ^{137}Ba), which possess nuclear spins (I = 3/2). These odd isotopes cause asymmetries and broadenings in the line profiles that are not present in even isotopes. By modeling the observed line shapes—including HFS components derived from laboratory measurements of magnetic dipole (A) and electric

quadrupole (B) constants—astronomers can disentangle the contributions of odd and even isotopes. The resulting best-fit synthetic spectrum yields an estimate of $f_{\text{odd,Ba}}$ [12].

The most rigorous work should encapsulate both HFS and isotopic shift (IS). However, the IS is often neglected due to its very difficult measurement from atomic lines, as the shift is negligible (often only a few mÅ) compared to the line width that is highly constrained by the instrumental resolution [11].

Using the Multiconfiguration Dirac–Hartree–Fock (MCDHF) method [13], as implemented in the General Relativistic Atomic Structure Package (GRASP) [14], our study extends the work of Itano [15] on the excited D levels of ^{137}Ba II and ^{87}Sr II. We focus on calculating the hyperfine structure constants for the ground as well as the first excited levels. To address the discrepancies identified by Itano [15] for the $A(^2D_{5/2})$ constant for these ions, we employ a comprehensive analysis using independent correlation models. Additionally, we benchmark the new code developments including natural orbitals and non-orthogonal orbital sets that explicitly account for polarization effects. This work is the first determination of HFS constants using the MCDHF method for the levels involved in the resonance lines of ^{87}Sr II and give additional theoretical values with an uncertainty determination for the $^2D_{3/2}$ and $^2P^o_{1/2}$ levels, where experimental data are unavailable. Finally, the developed correlation models are applied to the more complex system of ^{137}Ba I, aiming to refine earlier MCDHF theoretical results [16]. While this study does not simulate nucleosynthesis yields, the HFS constants provided in this study are essential input for stellar spectroscopy codes used to infer process-specific abundances. The statistical uncertainties quantified in our recommended values are critical for propagating errors in $f_{\text{odd,Ba}}$ determinations, which in turn constrain the dominant nucleosynthesis pathway.

The paper is structured as follows.In Section 2, the theoretical method used to determine the hyperfine structure constants of ^{135,137}Ba II, ^{137}Ba I, and ^{87}Sr II are presented as well as a in-depth study of correlation models and excitations. Then, in Section 3, the best results obtained for each element are discussed as new methods are tested. Finally, in Section 4, the key results and outlooks are given as a conclusion.

2. Methods

2.1. Multiconfiguration Dirac–Hartree–Fock Method

The Multiconfiguration Dirac–Hartree–Fock (MCDHF) method, as presented in Grant's book [13], is a fully relativistic approach to atomic structure, particularly suited for moderate-to-heavy elements and highly charged ions. It is a multiconfiguration method in a sense that the wave function of the atomic state $|\Gamma\pi JM_J\rangle$, with Γ being its identifying label, J as the total angular momentum quantum number of the polyelectronic system, M_J as the total magnetic quantum number, and π as the parity, is approximated by an Atomic State Function (ASF) Ψ, which is a linear combination of Configuration State Functions (CSFs) Φ

$$\Psi(\Gamma\pi JM_J) = \sum_{i=1}^{N_{\text{CSFs}}} c_i^{\Gamma\pi J}\Phi(\gamma_i\pi JM_J), \tag{2}$$

where γ_i specifies the electronic configuration, the coupling tree of angular momenta, and other quantum numbers needed to uniquely describe the CSF.

The $\{c_i^{\Gamma\pi J}\}$ set represents all the mixing coefficients that are determined, along with the total energy E, by solving the eigenvalue problem

$$\boldsymbol{Hc} = E\boldsymbol{c} \tag{3}$$

with $\boldsymbol{H}$ being the Hamiltonian matrix. By applying the variational principle on an energy functional, a system of coupled integro-differential equations, namely the MCDHF equa-

tions, is obtained for the radial parts of the spin-orbitals building the CSFs and solved using the self-consistent field iterative method.

2.2. Hyperfine Structure

The atomic property of interest in this paper is the hyperfine structure. The latter is related to the hyperfine structure constants, i.e., the magnetic dipole constant A and the electric quadrupole constant B. The hyperfine interaction can be expressed as a multipolar expansion given by

$$H_{\mathrm{HFS}} = \sum_{k\geq 1} \boldsymbol{T}^{(k)} \cdot \boldsymbol{M}^{(k)}, \tag{4}$$

where $\boldsymbol{T}^{(k)}$ and $\boldsymbol{M}^{(k)}$ are spherical tensor operators of rank k in the electronic and nuclear space, respectively, that represent the dipolar magnetic (M1) and quadrupole electric (E2) interactions when k is equal to 1 and 2, respectively. For an atom composed of N_e electrons, the $\boldsymbol{T}^{(k)}$ operators for $k = 1, 2$ are given by

$$\boldsymbol{T}^{(1)} = \sum_{j=1}^{N_e} \boldsymbol{t}^{(1)}(j) = \sum_{j=1}^{N_e} -i\sqrt{2}\alpha r^{-2}(\boldsymbol{\alpha}_j \cdot \boldsymbol{C}^{(1)}(\theta_j, \varphi_j)), \tag{5}$$

$$\boldsymbol{T}^{(2)} = \sum_{j=1}^{N_e} \boldsymbol{t}^{(2)}(j) = \sum_{j=1}^{N_e} -r_j^{-3}\boldsymbol{C}^{(2)}(\theta_j, \varphi_j). \tag{6}$$

The nuclear magnetic dipole moment μ_I and the electric quadrupole moment Q are defined through the matrix elements of the nuclear tensor operators $\boldsymbol{M}^{(k)}$ for $k = 1, 2$, respectively,

$$\mu_I = \langle II|M^{(1)}|II\rangle, \tag{7}$$

$$Q = 2\langle II|M^{(2)}|II\rangle, \tag{8}$$

with $\boldsymbol{M}^{(1)} \equiv \boldsymbol{\mu_I}$, $\boldsymbol{M}^{(2)} \equiv \boldsymbol{Q}^2$ being the electric quadrupole tensor and $|II\rangle$ being the nuclear state with the maximum component of the nuclear spin, $M_I = I$ [17].

If the hyperfine interaction is weak so that the interaction energy is small compared with the fine structure level splitting, the Hamiltonian (4) can be treated perturbatively. The first-order energy contribution is

$$E_{\mathrm{HFS}} = \langle \Gamma JIFM_F|H_{\mathrm{HFS}}|\Gamma JIFM_F\rangle = E^{\mathrm{M1}}_{\mathrm{HFS}} + E^{\mathrm{E2}}_{\mathrm{HFS}}, \tag{9}$$

where $|\Gamma IJFM_F\rangle$ is the zeroth-order wave function of the coupled state [18], and F and M_F are, respectively, the hyperfine structure total angular momentum and its projection along the quantization axis. In practice, the magnetic dipole A and the electric quadrupole B constants are factorized out for calculation, with

$$E^{\mathrm{M1}}_{\mathrm{HFS}} = \frac{1}{2}A_{\Gamma J}C \tag{10}$$

$$E^{\mathrm{E2}}_{\mathrm{HFS}} = B_{\Gamma J}\frac{\frac{3}{4}C(C+1) - I(I+1)J(J+1)}{2I(2I-1)J(2J-1)}, \tag{11}$$

where

$$A_{\Gamma J} = \frac{\mu_I}{I}\frac{1}{J(J+1)2(J+1)}\langle \Gamma J||\boldsymbol{T}^{(1)}||\Gamma J\rangle \tag{12}$$

$$B_{\Gamma J} = 2Q\sqrt{\frac{J(2J-1)}{(J+1)(2J+1)(2J+3)}}\langle \Gamma J||\boldsymbol{T}^{(2)}||\Gamma J\rangle, \tag{13}$$

and $C = F(F+1) - J(J+1) - I(I+1)$. The reduced matrix elements $\langle \Gamma J || \boldsymbol{O}^{(k)} || \Gamma J \rangle$, with $\boldsymbol{O}^{(k)} = \boldsymbol{T}^{(1)}$ or $\boldsymbol{T}^{(2)}$, are computed using the ASFs through the GRASP package [14].

2.3. Computational Details

The hyperfine structure constants were calculated using the GRASP package, first introduced by Dyall et al. [19], in a systematic manner using the latest GRASP2018 version [14], where all application programs are described in [20]. To speed up the calculations, the new code GRASPG developed by Si et al. [21], using the powerful Configuration State Function Generators (CSFGs), has been employed for the configuration interaction part of the work.

Following the ideas of Papoulia et al. [22], we derive recommended hyperfine structure (HFS) constants for each studied level by treating the results of the largest Relativistic Configuration Interaction (RCI) calculations, employing distinct optimization strategies, as a set of independent values. This statistical approach enables us to give a mean value and a standard deviation to the calculated constants, thereby providing a robust estimate of the HFS constants, crucial when there is no experimental data. The recommended values are presented in the form $\mu \pm 2\sigma$, corresponding to a 95% confidence interval. Further details, including the specific optimization strategies and statistical analyses, are provided for each studied ion.

3. Results and Discussion

3.1. Ba II

Barium ($Z = 56$) has 40 known isotopes, but only 8 of them are stable and 7 are natural. Because astrophysicists are interested in the odd isotopes for the determination of $f_{\mathrm{odd,Ba}}$, only the $A = 135$, 137 nuclei are considered in this paper. Moreover, only 5 levels have been studied—3 even levels ($[Xe]6s\ ^2S_{1/2}$, $[Xe]5d\ ^2D_{3/2,5/2}$) and 2 odd levels ($[Xe]6p\ ^2P^o_{1/2,3/2}$)—as the S and P levels are very often used for abundance calculations when studying the resonance lines. The D levels are also of interest because more accurate atomic data could help astrophysicists in their determination of abundances thanks to the secondary lines.

For these levels, theoretical studies have already been conducted by Sahoo et al. [23] using the Relativistic Coupled Cluster (RCC) method, as well as by Safronova [24] applying the Relativistic Many-Body Perturbation Theory (RMBPT). Itano's work [15] is of particular interest as he used the MCDHF method, the same one used for our calculations. These theoretical results are compared with experimental values obtained by laser-induced hyperfine transition spectroscopy [25–28].

The Active Set (AS) [18] and the layer-by-layer [20] approaches have been considered. These approaches are useful for the study of heavy elements as only a small portion of orbitals needs to be optimized at each step of the calculation. Let us take the concrete example of the ground level $^2S_{1/2}$ of ^{137}Ba II for which a single reference (SR) is used for defining the zero-order set of CSFs from which orbital substitutions are considered. The first layer in the AS approach is the Dirac–Hartree–Fock (DHF) one, based on the spectroscopic orbitals. For instance, the $[Xe]6s\ ^2S_{1/2}$ level has the $\{6s, 5p, 4d\}$ AS, in the non-relativistic notation, where the largest n quantum number is quoted for each ℓ-symmetry. For each selected AS, the hyperfine structure constants are evaluated with the corresponding MCDHF wave function. The AS is progressively enlarged by considering more correlation orbitals, with the hope of achieving the convergence of the considered atomic property, within some a priori accepted variation interval. The increasing ASs are given in Table 1 for the different levels considered in the present study. The choice of restricting the ASs to $\ell_{max} = 4$ (g-orbitals) can be justified by the fact that the orbitals having a higher angular momentum

are located further away from the nucleus; therefore, they do not significantly contribute to the hyperfine structure constants [29].

Table 1. Considered active sets used for the levels studied in ^{135,137}Ba II.

Correlation Layer	$^2S_{1/2}$	$^2D_{3/2,5/2}$	$^2P^o_{1/2,3/2}$
DHF (SR)	$\{6s, 5p, 4d\}$	$\{5s, 5p, 5d\}$	$\{5s, 6p, 4d\}$
AS1	$\{7s, 6p, 5d, 4f\}$	$\{6s, 6p, 6d, 4f\}$	$\{6s, 7p, 5d, 4f\}$
AS2	$\{8s, 7p, 6d, 5f, 5g\}$	$\{7s, 7p, 7d, 5f, 5g\}$	$\{7s, 8p, 6d, 5f, 5g\}$
AS3	$\{9s, 8p, 7d, 6f, 6g\}$	$\{8s, 8p, 8d, 6f, 6g\}$	$\{8s, 9p, 7d, 6f, 6g\}$
AS4	$\{10s, 9p, 8d, 7f, 7g\}$	$\{9s, 9p, 9d, 7f, 7g\}$	$\{9s, 10p, 8d, 7f, 7g\}$
AS5	$\{11s, 10p, 9d, 8f, 8g\}$	$\{10s, 10p, 10d, 8f, 8g\}$	$\{10s, 11p, 9d, 8f, 8g\}$
AS6	$\{12s, 11p, 10d, 9f, 9g\}$	$\{11s, 11p, 11d, 9f, 9g\}$	$\{11s, 12p, 10d, 9f, 9g\}$
AS7	$\{13s, 12p, 11d, 10f, 10g\}$	$\{12s, 12p, 12d, 10f, 10g\}$	$\{12s, 13p, 11d, 10f, 10g\}$

The choice of substitutions to include in the correlation models is the key to obtain reliable estimations of atomic parameters with the MCDHF method. It can been seen from Equations (5) and (6) that the hyperfine structure constants involve one-electron operators only. Therefore, the CSFs generated from single (S) substitutions are the most important, and they are included in the single and restricted double (SrD) substitution strategies, where restricted means that there is at most one hole in the active core orbitals (e.g., [30]). Moreover, according to non-relativistic atomic physics [31], the s electrons have a non-zero probability of presence in the nucleus. Electronic substitutions from these are therefore important for the HFS and an optimization strategy based on SrD substitutions involving the most important s orbitals is a natural choice.

Inspired by the work of Bieroń et al. [32], the impact of different classes of orbital substitutions has been studied for the ground and first excited levels in ^{137}Ba II. Using an orbital basis that has been optimized with SrD substitutions from the 5s, 5p core-, and the 6s valence- orbitals, with at most one substitution of the core orbitals, more correlation excitations are accumulated by allowing single and double (SD) substitutions from deeper orbitals, using the multireference (MR) ($[Xe]6s + [Xe]5d$) for the even parity and the single reference (SR) $[Xe]6p$ for the odd parity. Figure 1 shows the different contributions of single (S) substitutions to the magnetic dipole hyperfine constant $A(^2S_{1/2})$. Double (D) substitutions were also investigated but, as shown by Bieroń et al. [32], their contribution is much smaller.

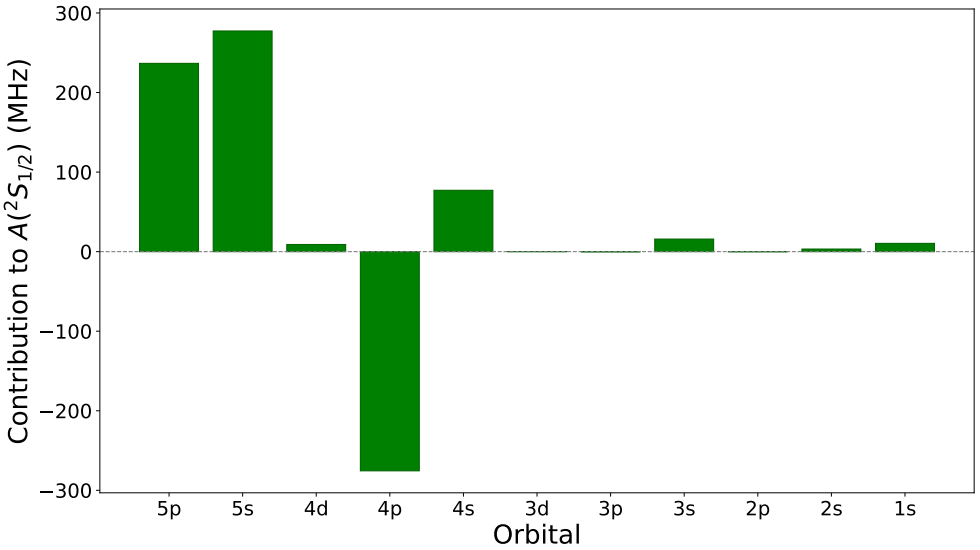

Figure 1. Contributions of single (S) orbital substitutions relative to the DHF $A(^2S_{1/2})$ constant in ^{137}Ba II.

This analysis illustrates that most of the one-electron orbital substitutions increase the $A(^2S_{1/2})$ constant. The contributions of the $4s, 3s, 2s$ and $1s$ single substitutions confirm their importance for the HFS. Nevertheless, the adopted optimization strategy limits the orbital substitutions to the outer occupied subshells as deep as the $4p$ orbital, even if the ns, $n = 1, 2, 3, 4$ orbitals are a priori relevant. The validity of this restriction was assessed for the $[Xe]6s\ ^2S_{1/2}$ level by observing that the sum of the S substitution contributions from those core orbitals was less than 1%. The same strategy has been adopted for the excited levels as those contributions were even smaller than for the ground level. According to Yuan et al. [33], the $p_{1/2}$ core electrons can also make non-vanishing exchange core polarization contributions in the relativistic theory. This is confirmed by the rather large negative contribution of the single substitutions of the $4p$ orbital ($\simeq -300$ MHz).

Thanks to this analysis, the optimization of the radial orbitals is focused on core–valence (CV) correlations. A stepwise approach was used for the ground $^2S_{1/2}$ level, but for conciseness, the reported results are limited to those obtained with two selected optimization schemes. Using the AS described in Table 1, the first one allows SrD substitutions as deep as the $5s$ orbital, in order to include the two important contributions from $5p$ and $5s$ orbitals, as seen in Figure 1. According to this figure, another interesting strategy is the one allowing SrD substitutions as deep as the $4p$ orbital, even if its contribution is to decrease the A constant value. The corresponding results are given in Table 2, under the labels CV SrD $nl \geq 5s$ and $nl \geq 4p$, respectively.

Considering the ground level, we can see that the hyperfine constant values become stable at the level of AS5 for both optimization strategies. The calculations have been extended up to AS7 to manage the convergence with a larger number of correlation orbitals and in order to monitor the Relativistic Configuration Interaction (RCI) calculations that follow the orbital optimization MCDHF calculations. The first optimization strategy, CV SrD $nl \geq 5s$, gives promising results, with an A constant value approaching the experimental value within 55 MHz for AS7. The second strategy, CV SrD $nl \geq 4p$, overestimates the experimental value by about 400 MHz for AS7.

For the excited levels, a similar behavior is observed, with a stable value achieved for AS5, in great agreement with experimental values for the first optimization strategy and an overestimation for the second one. For example, the D levels results show that the CV SrD $nl \geq 5s$ approach better suits the A hyperfine constants, with 5% and 16% for the $^2D_{3/2}$ and $^2D_{5/2}$ levels, respectively, but not the B constants, for which a large theory–observation discrepancy ($\simeq 41\%$) is observed for both levels. Adding more correlations in the CV SrD $nl \geq 4p$ model improves the agreement with experiment for the B hyperfine constants, within less than a MHz for both of the D levels. This comes with a high price to pay: the A theoretical constants overestimate the experimental values by up to 80% for the $^2D_{5/2}$ level. When the computations were undertaken, this behavior was unknown, as Itano's MCDHF work [15] did not mention any of these observations. We believe that adding correlation orbitals with higher l encapsulates the orbital polarization that was neglected and is important for a reliable determination of the B hyperfine constant [17].

Table 2. Magnetic dipole A and electric quadrupole B hyperfine structure constants (in MHz) of ^{137}Ba II ($I = 3/2, \mu = 0.9375\mu_N, Q = 0.236$ b [34]), compared to available theoretical and experimental data. The recommended values are given in the form of $\mu \pm 2\sigma$, exhibiting a 95% confidence level. *: Number of CSFs obtained after reduction using the rcsfginteract_csfg code [a]: Th. Sahoo et al. (RCC) [23]; [b]: Th. Safronova (RMBPT) [35]; [c]: Th. Itano (MCDHF) [15]; [d]: Expt. Blatt & Werth [25]; [e]: Expt. Silverans et al. [26]; [f]: Expt. Villemoes et al. [27].

Step	$^2S_{1/2}$		$^2D_{3/2}$			$^2D_{5/2}$			$^2P^o_{1/2}$		$^2P^o_{3/2}$		
	N_{CSFs}	A	N_{CSFs}	A	B	N_{CSFs}	A	B	N_{CSFs}	A	N_{CSFs}	A	B
Optimization CV SrD $nl \geq 5s$													
DHF	1	3060	1	132	33	1	53	42	1	540	1	80	59
MCDHF (+AS1)	54	3735	120	180	20	130	−24	26	74	655	117	95	78
MCDHF (+AS2)	217	3885	433	177	27	496	−19	36	250	689	417	125	83
MCDHF (+AS3)	494	3992	944	181	26	1100	−17	35	542	715	919	125	86
MCDHF (+AS4)	885	3963	1653	179	27	1942	−14	36	950	716	1623	122	85
MCDHF (+AS5)	1390	3974	2560	180	27	3022	−15	35	1474	719	2529	122	86
MCDHF (+AS6)	2009	3963	3665	179	27	4340	−14	35	2114	717	3637	122	86
MCDHF (+AS7)	2742	3964	4968	180	27	5896	−14	35	2870	716	4947	122	85
RCI CC SD $nl \geq 5s$ (+AS7)	12,385	3636	27,462 *	165	30	38 541 *	−9	40	11,173 *	623	26,620 *	106	75
RCI CC SD $nl \in \{5p, 5s, 4p, 4s\}$ (+AS7)	24,762	3773	54,916 *	168	39	77,074 *	−3.82	52	22,338 *	643	52,232 *	116	80
Optimization CV SrD $nl \geq 4p$													
DHF	1	3060	1	132	33	1	53	42	1	540	1	80	59
MCDHF (+AS1)	135	3823	321	186	26	355	−22	34	183	696	196	98	80
MCDHF (+AS2)	572	4114	1182	202	43	1374	−9	58	660	722	1122	130	89
MCDHF (+AS3)	1323	4382	2597	214	43	3069	−6	58	1453	814	2504	136	99
MCDHF (+AS4)	2388	4364	4566	215	46	5437	−2	61	2562	826	4442	136	100
MCDHF (+AS5)	3767	4414	7089	216	45	8479	−3	60	3987	837	6936	138	101
MCDHF (+AS6)	5460	4409	10,166	215	46	12,195	−2	61	5728	837	9986	137	101
MCDHF (+AS7)	7467	4412	13,797	216	46	16,585	−2	61	7785	837	13,592	138	101
RCI CC SD $nl \geq 5s$ (+AS7)	17,110	3972	36,291 *	195	47	49,230 *	1	62	16,088 *	712	35,265 *	117	87
RCI CC SD $nl \in \{5p, 5s, 4p, 4s\}$ (+AS7)	27,513	4031	60,116 *	189	46	83,458 *	5	62	25,147 *	692	58,232 *	120	85
This work, recommended		3902 ± 364		179 ± 29	43 ± 11		1 ± 12	57 ± 14		667 ± 69		118 ± 6	82 ± 8
Th. [a]		4078		190	46		−12	62		741		128	93
Th. [b]		3997		192	46		−10	61		734		121	93
Th. [c]				193	51		9	68					
Expt.		4018.87 ± 0.18 [d]		189.7288 ± 0.0006 [e]	44.54 ± 0.16 [e]		-12.028 ± 0.011 [e]	59.533 ± 0.043 [e]		743.7 ± 0.3 [f]		127.2 ± 0.2 [f]	92.5 ± 0.2 [f]

After the MCDHF optimization step, more correlations can be added in Relativistic Configuration Interaction (RCI) calculations. As it has been shown in the literature [36], higher-order correlations are important for the HFS. Even if H_{HFS} (4) only contains one-electron tensor operators, the inclusion of single and non-restricted double (SD) substitutions leads to a rearrangement of mixing coefficients [37]. Core–core (CC) correlations are therefore added to the model. Two RCI strategies were tested on the basis of the two considered optimization strategies. These calculations showed that the hyperfine constants are very sensitive to the correlation model. Ultimately, the more correlations the better, with CC SD $nl \in \{5p, 5s, 4p, 4s\}$ substitutions added to the CV SrD $nl \geq 4p$ optimization, giving a value as close as 0.3% ($\approx$12 MHz) to the experimental value for the ground level. CC correlation excitations from deeper p or s orbitals were found to be negligible for the HFS. This result is consistent with the conclusions drawn by the study of Figure 1.

The same RCI strategy has been applied to the excited levels. The P levels hyperfine constants are still underestimated, but agree satisfactorily (<10%) with the experimental values. Results for the D levels are accurate within less than 2 MHz for all constants. However, the $A(^2D_{5/2})$ constant differs from the experimental value by more than 140%. This behavior was already observed by Itano [15] while using MCDHF. However, other theoretical methods, such as RCC or RMBPT, do not face such an issue. As far as the MCDHF/RCI method is concerned, the agreement with observation of the theoretical values of the present work is systematically better than the one found by Itano [15].

As detailed in Section 2.3, the recommended values for the hyperfine structure (HFS) constants are presented in the $\mu \pm 2\sigma$ format, reflecting a 95% confidence interval. The optimization of the radial components of the spin-orbitals depends critically on the electronic configuration. The recommended values explicitly highlights the differences arising from the choice of orbital basis set. An optimization strategy limited to the 5s electrons yields more accurate results for the magnetic dipole constant A. In contrast, the electric quadrupole constant B is better described when deeper correlations (up to 4p electrons) are included. Consequently, no single optimization strategy universally applies to both constants. This distinction is seen in the recommended values, where a 2σ uncertainty range is employed to assess the sensitivity of each constant to the chosen optimization approach.

Several studies have proposed improved methods for calculating the hyperfine structure (HFS) constants of different atomic species. Li et al. [38] and Ma et al. [29] investigated the role of polarization orbitals in light of Li and N elements. A similar analysis was carried out for ^{137}Ba II with the GRASPG package that allowed more flexibility for the relabeling, and it yielded promising results. The A constants of the $^2S_{1/2}$ and $^2D_{3/2}$ levels increased by about 200 MHz and 4 MHz, respectively, regardless of the computational strategy used (MCDHF CV SrD $nl \geq 5s$ + RCI CC SD $nl \geq 5s$, or MCDHF CV SrD $nl \geq 4p$ + RCI CC SD $nl \in \{5p, 5s, 4p, 4s\}$). For the $^2D_{5/2}$ level, the A constant decreased by 2 MHz (from -9 to -12 MHz) with the first strategy, reaching a negligible 0.2% difference with the experimental value. This decreasing trend was also observed with the second, more complete strategy, although the reduction was smaller and could not entirely solve the $A(^2D_{5/2})$ problem. In contrast, the B constants of the D levels were barely affected by the polarization orbitals. These results are encouraging, but difficult to obtain in practice. The artificially enlarged orbital sets and the moving ASF labels indeed require a careful and time-consuming study. With the available computational resources and time, it was not possible to fully monitor the convergence of the calculations.

In the layer-by-layer approach [20] used for the MCDHF calculations, only the newly introduced orbitals are optimized at each step, while the others remain frozen to avoid the numerical instability issues often encountered when allowing all the orbitals to be variational. Natural orbitals (NOs) provide an alternative basis for studying the HFS. Originally

developed in quantum chemistry to account for electron correlation in molecules [39,40], they were later introduced in atomic physics by Lindgren et al. [41] for perturbative treatments of the HFS. More recently, Schiffmann et al. [42] extended the NO formalism to the MCDHF framework in GRASP using the rdensity program. Their work on Na I [43] demonstrated that relaxing frozen orbitals significantly affects the HFS constants. A similar study on ^{137}Ba II has been performed. After the RCI steps, the orbital basis is transformed and the calculations are performed again. This showed a systematic increase in both A and B constants across all levels considered in the MCDHF CV SrD $nl \geq 4p$ + RCI CC SD $nl \in \{5p, 5s, 4p, 4s\}$ strategy. This trend is consistent with the Na I results. However, the case of the $A(^2D_{5/2})$ constant was not resolved. The calculated value increased from 5 to 7 MHz, resulting in a discrepancy of about 160% with the experimental value.

Finally, allowing triple (T) substitutions in HFS calculations has been shown to correct CC correlation effects in ^{109}Cd I–II [44], an element similar to ^{137}Ba I–II with an outer s shell. For ^{137}Ba II, only a limited subset of T substitutions could be included, since the number of CSFs grows very rapidly with respect to the increasing orbital set. Nevertheless, the inclusion of substitutions improved the HFS constants for the odd P levels.

As hyperfine structure constants values are needed for different odd isotopes to compute $f_{\text{odd,Ba}}$ that can be used by astrophysicists, the ^{135}Ba II values were calculated from the MCDHF CV SrD $nl \geq 4p$ + RCI CC SD $nl \in \{5p, 5s, 4p, 4s\}$ ones from ^{137}Ba II calculations in Table 2, employing appropriate scaling with the nuclear magnetic dipole μ and electric quadrupole Q moments for ^{135}Ba [22] taken from IAEA's database [34].

While Mårtensson-Pendrill et al. [45] used the RCC method in a traditional way, the results given by Sahoo et al. [46] were obtained by computing B/Q values. The Q values were extracted from experimental data and were compared to the theoretical ones for different levels, and different isotopes for consistency checks. A new study from Cserveny & Roberts [47] was not known by the time all the present calculations were finished. However, their results are given in Table 3 in order to compare our MCDHF results with their Atomic Many-body Perturbation theory in the Screened Coulomb Interaction (AMPSCI). These theoretical results are also compared with the experimental values of Wendt et al. [28] for the $^2S_{1/2}$ level, Silverans et al. [26] for the excited $^2D_{3/2,5/2}$ levels and Villemoes et al. [27] for the $^2P^o_{1/2,3/2}$ levels, all obtained using the collinear laser-ion beam spectroscopy technique. The calculated values for ^{135}Ba II using the approach described above are reported in Table 3 for the five considered levels, with an estimation of the uncertainty on our recommended values.

Table 3. Magnetic dipole A and electric quadrupole B hyperfine structure constants (in MHz) of ^{135}Ba II ($I = 3/2, \mu = 0.8381\mu_N, Q = 0.153$ b [34]), compared to available theoretical and experimental data. The recommended values are given in the form of $\mu \pm 2\sigma$, exhibiting a 95% confidence level. [a]: Th. Mårtensson-Pendrill et al. (RCC) [45]; [b]: Th. Cserveny & Roberts (AMPSCI) [47]; [c]: Th. Sahoo et al. (RCC) [46]; [d]: Expt. Wendt et al. [28]; [e]: Expt. Silverans et al. [26]; [f]: Expt. Villemoes et al. [27].

Level	*A*				*B*		
	This Work	**Th.** [a]	**Th.** [b]	**Expt.**	**This Work**	**Th.** [c]	**Expt.**
$^2S_{1/2}$	3469 ± 338	3595	3595 ± 19	3593.3 ± 2.2 red [d]	/	/	/
$^2D_{3/2}$	159 ± 27	190	190 ± 18	169.5892 ± 0.0009 [e]	28 ± 7	29	28.9536 ± 0.0025 [e]
$^2D_{5/2}$	2 ± 11	-14	-14 ± 17	-10.735 ± 0.002 [e]	37 ± 10	39	38.688 ± 0.010 [e]
$^2P^o_{1/2}$	596 ± 67	673	673 ± 92	664.5 ± 0.3 [f]	/	/	/
$^2P^o_{3/2}$	105 ± 8	113	113 ± 88	113.0 ± 0.1 [f]	53 ± 6	58	59.0 ± 0.1 [f]

The latter are in good agreement with experiment, with discrepancies of approximately 4% for the ground level and less than 5% for the computed B hyperfine structure constants of D levels. However, a high discrepancy between theory and experiment ($\simeq$120%) persists for the $A(^2D_{5/2})$ constant, to be compared with the 6% found for the $^2D_{3/2}$ level. The present theoretical values of the HFS constants of the P levels do agree reasonably well with observation, with discrepancies ranging from 7% to 10%. While the results of Cserveny & Roberts [47] appear to be in better agreement for all levels except for the A hyperfine structure constants of the D levels, their values carry high uncertainties that cover our calculated MCDHF values.

3.2. Sr II

The second test case of the applicability of the model developed for ^{137}Ba II is ^{87}Sr II, a lighter alkali-like ion with a similar electronic configuration. The levels of interest are similar to the ones considered in ^{137}Ba II, i.e., $[Kr]5s\ ^2S_{1/2}$, $[Kr]4d\ ^2D_{3/2,5/2}$ for the even parity, and $[Kr]5p\ ^2P^o_{1/2,3/2}$ for the odd parity. The hyperfine structure constants have already been computed in the literature. Theoretical values using the RMBPT [35] or MCDHF [15] approaches are aiming to reproduce the experimental results obtained using laser-microwave double resonance spectroscopy [48,49] or via collinear fast beam laser spectroscopy [50].

For the five considered levels, the ASs are given in Table 4 and are similar to the ones used in ^{137}Ba II calculations.

Table 4. Considered active sets used for the levels studied in ^{87}Sr II.

Correlation Layer	$^2S_{1/2}$	$^2D_{3/2,5/2}$	$^2P^o_{1/2,3/2}$
DHF	$\{5s,4p,3d\}$	$\{4s,4p,4d\}$	$\{4s,5p,3d\}$
AS1	$\{6s,5p,4d,4f\}$	$\{5s,5p,5d,4f\}$	$\{5s,6p,4d,4f\}$
AS2	$\{7s,6p,5d,5f,5g\}$	$\{6s,6p,6d,5f,5g\}$	$\{6s,7p,5d,5f,5g\}$
AS3	$\{8s,7p,6d,6f,6g\}$	$\{7s,7p,7d,6f,6g\}$	$\{7s,8p,6d,6f,6g\}$
AS4	$\{9s,8p,7d,7f,7g\}$	$\{8s,8p,8d,7f,7g\}$	$\{8s,9p,7d,7f,7g\}$
AS5	$\{10s,9p,8d,8f,8g\}$	$\{9s,9p,9d,8f,8g\}$	$\{9s,10p,8d,8f,8g\}$
AS6	$\{11s,10p,9d,9f,9g\}$	$\{10s,10p,10d,9f,9g\}$	$\{10s,11p,9d,9f,9g\}$
AS7	$\{12s,11p,10d,10f,10g\}$	$\{11s,11p,11d,10f,10g\}$	$\{11s,12p,10d,10f,10g\}$

Applying to ^{87}Sr II the computational strategy developed for ^{137}Ba II yields the results presented in Table 5. The latter demonstrates the great direct applicability of the MCDHF CV SrD $nl \geq 4p$ + RCI CC SD $nl \in \{5p,5s,4p,4s\}$ model. The hyperfine structure constants are indeed well reproduced, with, for example, 14 MHz for the $A(^2S_{1/2})$ constant. However, while this strategy looks reliable for the $A(^2D_{3/2})$ constant in ^{137}Ba II, there remains a large disagreement with other theoretical results ($\approx$50%) for ^{87}Sr II. Additionally, the problematic behavior previously observed for the $A(^2D_{5/2})$ constant persists.

Not only does the recommended value exhibit the difficulty to use a single optimization scheme for both A and B constants, but it also gives a robust value for astrophysicists with an uncertainty evaluation, where there is no experimental values, such as in the $^2D_{3/2}$ and $^2P^o_{1/2}$ levels. The recommended values for this work are in satisfactory agreement with experiments and available theoretical data, while reproducing Itano's [15] discrepancy for the $A(^2D_{5/2})$ constant. Such as in the ^{137}Ba II, this smallest value for the five studied levels is the most sensitive to the orbital basis change. To understand this, we investigate the magnetic dipole hyperfine structure constant of $4d\ ^2D_{3/2,5/2}$ based on the non-relativistic formalism for which the hyperfine interaction constants are given as the sum of the orbital, spin-dipolar and Fermi contact terms [31]. An initial Hartree–Fock (HF) calculation yields the terms at the top in Table 6.

Table 5. Magnetic dipole A and electric quadrupole B hyperfine structure constants (in MHz) of ^{87}Sr II ($I = 9/2, \mu = -1.09316\mu_N, Q = 0.305$ b [34]), compared to available theoretical and experimental data. The recommended values are given in the form of $\mu \pm 2\sigma$, exhibiting a 95% confidence level. *: Number of CSFs obtained after reduction using the rcsfginteract_csfg code; [a]: Th. Safronova (RMBPT) [35]; [b]: Th. Itano (MCDHF) [15]; [c]: Expt. Suanoshi et al. [48]; [d]: Expt. Barwood et al. [49]; [e]: Expt. Buchinger et al. [50].

Step	$^2S_{1/2}$		$^2D_{3/2}$			$^2D_{5/2}$			$^2P^o_{1/2}$		$^2P^o_{3/2}$		
	N_{CSFs}	A	N_{CSFs}	A	B	N_{CSFs}	A	B	N_{CSFs}	A	N_{CSFs}	A	B
Optimization CV SrD $nl \geq 4s$													
DHF	1	−761	1	−32	25	1	−13	35	1	−132	1	−23	55
MCDHF (+AS1)	54	−928	120	−43	17	130	3	23	74	−156	117	−28	74
MCDHF (+AS2)	217	−967	433	−45	24	496	2	33	250	−169	417	−36	79
MCDHF (+AS3)	494	−996	944	−46	24	1100	2	33	542	−174	919	−37	81
MCDHF (+AS4)	885	−989	1653	−45	24	1942	1	34	950	−174	1623	−36	80
MCDHF (+AS5)	1390	−992	2560	−46	24	3022	1	34	1474	−175	2529	−36	81
MCDHF (+AS6)	2009	−991	3665	−46	24	4340	1	33	2114	−175	3637	−36	81
MCDHF (+AS7)	2742	−990	4968	−46	24	5896	1	33	2870	−174	4947	−36	81
RCI CC SD $nl \geq 4s$ (+AS7)	10,727 *	−913	27,462 *	−58	36	38,541 *	−3	47	11,173 *	−152	26,620 *	−31	71
RCI CC SD $nl \in \{4p, 4s, 3p, 3s\}$ (+AS7)	21 446 *	−948	54,916 *	−41	32	77,074 *	−1	45	22,338 *	−158	53,232 *	−34	76
Optimization CV SrD $nl \geq 3p$													
DHF	1	−761	1	−32	25	1	−13	35	1	−132	1	−23	55
MCDHF (+AS1)	135	−931	321	−44	20	355	3	28	183	−159	296	−28	76
MCDHF (+AS2)	572	−985	1182	−48	35	1375	0	49	660	−173	1122	−37	82
MCDHF (+AS3)	1323	−1043	2597	−53	37	3069	0	52	1453	−190	2504	−39	90
MCDHF (+AS4)	2388	−1049	4566	−54	40	5437	−2	54	2562	−194	4442	−39	91
MCDHF (+AS5)	3767	−1057	7089	−55	38	8479	−2	52	3987	−196	6936	−40	92
MCDHF (+AS6)	5460	−1058	10,166	−55	38	12,195	−2	53	5728	−196	9986	−40	92
MCDHF (+AS7)	7467	−1059	13,797	−55	38	16,585	−2	53	7785	−196	13,592	−40	92
RCI CC SD $nl \geq 4s$ (+AS7)	15,452 *	−967	36,291 *	−48	38	49,230 *	−2	53	16,088 *	−169	35,265 *	−34	80
RCI CC SD $nl \in \{4p, 4s, 3p, 3s\}$ (+AS7)	24,197 *	−984	60,126 *	−23	37	83,458 *	−2	52	25,147 *	−165	58,232 *	−35	80
This work, recommended		-966 ± 51		-32 ± 26	35 ± 7		-2 ± 1	49 ± 10		-161 ± 10		-35 ± 1	78 ± 6
Th. [a]		−998		−47	37		2	52		−177		−35	89
Th. [b]				−46	41		−3	57					
Expt. [c]		-1000.4737 ± 0.0011											
Expt. [d]							2.1743 ± 0.0014	49.11 ± 0.06					
Expt. [e]		-1000.5 ± 1.0										-36.0 ± 0.4	88.5 ± 5.4

Table 6. M1 hyperfine interaction constants A in MHz for $4d\,^2D_{3/2,5/2}$ in ^{87}Sr II. The results at the top are from a HF calculation and the individual contributions from the orbital, spin-dipolar, and Fermi contact terms are shown along with the total value. The results at the bottom are the corresponding values from an MCHF calculation, including CV correlation based on one layer of correlation orbitals.

Level	Term Contribution			
	Orbital	Spin-Dipolar	Contact	Total A
		HF		
$^2D_{3/2}$	−26.7	−8.9	0.0	−35.7
$^2D_{5/2}$	−17.8	2.5	0.0	−15.3
		MCHF CV		
$^2D_{3/2}$	−19.9	−3.7	−14.6	−38.2
$^2D_{5/2}$	−13.3	1.1	14.6	2.4

We see that the Fermi contact term is zero for both states. At the lines below come the Multiconfiguration Hartree–Fock (MCHF) CV results, opening 4*s* and 4*p* for substitutions to one layer of correlation orbitals $\{5s, 5p, 5d\}$. For the calculations including CV correlation, we see a positive interference with the contact term for the $J = 3/2$ level and a negative interference for the $J = 5/2$ one, explaining the smallness of this constant as well as the difficulties in getting it correct. Obviously, a small imbalance in the large and canceling contributions due to an incomplete orbital basis and/or the neglect of higher-order correlation has a large impact on the total hyperfine interaction constant [51]. Even if the A constant is given by an operator with only one term in relativistic theory, there is a similar internal cancellation in MCDHF as in MCHF, explaining why it is so hard to obtain the hyperfine interaction constant right. The coupled cluster and RMBPT theories manage to balance the terms better due to the completeness of the basis, but also due to the fact that they contain non-linear terms corresponding to triple and higher-level excitations [52].

The natural orbitals (NOs) transformation was also investigated for the MCDHF CV SrD $nl \geq 4p$ + RCI CC SD $nl \in \{5p, 5s, 4p, 4s\}$ strategy for ^{87}Sr II and showed an increase in the positive values, as well as a decrease in the negative values. Similarly to the ^{137}Ba II case, this approach could not solve the problem of the $A(^2D_{5/2})$ and even worsens it.

3.3. Ba I

The last test of the applicability of the developed model in ^{137}Ba II is performed in neutral barium, ^{137}Ba I, an atomic system with one more *s* valence electrons. Therefore, MCDHF calculations should be performed by taking into consideration the valence–valence (VV) correlations. However, we already observed from the present Ba II study that the core–valence (CV) correlations are key to the model. It is therefore interesting to compare the obtained results when including and omitting the CV correlations in the optimization step. The first levels that have an hyperfine splitting are the excited $[Xe]6s5d\ ^1D_2$, $^3D_{1,2}$ and $[Xe]6s6p\ ^{1,3}P^o_1$ ones, as the ground level has a $J = 0$ value. The HFS constants have already been calculated in the literature. Theoretical calculations are performed using Dirac–Fock or Multiconfigurational Dirac–Fock [16], RCC [53], or RMBPT [54] methods and aim to reproduce the experimental results gathered in multiple studies with different experimental setups: interaction of an atomic beam with a magnetic field and a radio-frequency radiation [55,56], optical techniques [57], or induced hyperfine transitions using lasers [58].

In order to monitor the effect of adding VV correlations, multiple optimizations, using a SR or a MR, have been made with the ASs given in Table 7. While the SR only contains the configuration of interest, the MR for the *D* and the *P* levels were enlarged by a single

extra configuration, namely $[Xe]5d^2$ and $[Xe]6p5d$, respectively. These configurations were found to be crucial in estimating the hyperfine structure constants of ^{137}Ba I. One way to identify them is to use the rcsfmr program [20], which relies on the squared expansion coefficients of the LSJ-coupled CSFs, on a VV+CV correlations model. Setting a cut-off weight of 95% in the eigenvector composition gives the configurations that contribute by at least 5% and can be added to the MR. Including additional configurations beyond these two was found to be computationally inefficient, as it induced only negligible changes in the hyperfine structure constants.

Table 7. Considered active sets used for the studied levels in ^{137}Ba I.

Correlation Layer	$^1D_2$, $^3D_{1,2}$		$^1P^o_1$, $^3P^o_1$	
	SR	**MR**	**SR**	**MR**
DHF	$\{6s,5p,5d\}$	$\{6s,5p,5d\}$	$\{6s,6p,4d\}$	$\{6s,6p,5d\}$
AS1	$\{7s,6p,6d,4f\}$	$\{7s,6p,6d,4f\}$	$\{7s,7p,5d,4f\}$	$\{7s,7p,6d,4f\}$
AS2	$\{8s,7p,7d,5f,5g\}$	$\{8s,7p,7d,5f,5g\}$	$\{8s,8p,6d,5f,5g\}$	$\{8s,8p,7d,5f,5g\}$
AS3	$\{9s,8p,8d,6f,6g\}$	$\{9s,8p,8d,6f,6g\}$	$\{9s,9p,7d,6f,6g\}$	$\{9s,9p,8d,6f,6g\}$
AS4	$\{10s,9p,9d,7f,7g\}$	$\{10s,9p,9d,7f,7g\}$	$\{10s,10p,8d,7f,7g\}$	$\{10s,10p,9d,7f,7g\}$
AS5	$\{11s,10p,10d,8f,8g\}$	$\{11s,10p,10d,8f,8g\}$	$\{11s,11p,9d,8f,8g\}$	$\{11s,11p,10d,8f,8g\}$
AS6	$\{12s,11p,11d,9f,9g\}$	$\{12s,11p,11d,9f,9g\}$	$\{12s,12p,10d,9f,9g\}$	$\{12s,12p,11d,9f,9g\}$
AS7	$\{13s,12p,12d,10f,10g\}$	$\{13s,12p,12d,10f,10g\}$	$\{13s,13p,11d,10f,10g\}$	$\{13s,13p,12d,10f,10g\}$

The results given in Table 8 were produced adopting different optimization and configuration interaction strategies, considering a single- (SR) or a multireference (MR) set. Three orbital-optimization strategies and their associated RCI were considered. The first one, including only the VV correlations, is clearly underestimating the experimental values for the A hyperfine constants. The B constants are in good agreement with experiment for two out of three D levels, and underestimated for the P levels. This is not surprising as the hyperfine interaction is strongly affected by core–valence electron correlation. The second optimization scheme adds CV SrD $nl \geq 5s$ to the VV correlations. The corresponding results are in better agreement with the experimental values for all considered levels. The final optimization strategy digs deeper into the core with CV SrD $nl \geq 4p$ added to VV SD + CV SrD $nl \geq 5s$ correlations. Just like ^{137}Ba II, some values are far away from experiment, like the $^3D_{1,2}$ constants. The orbitals resulting from the last two optimization strategies are the most promising when looking at the MCDHF results.

Moving to RCI calculations as those performed for ^{137}Ba II ultimately led to promising results. Observations made for ^{137}Ba II also apply consistently to Ba I: (i) a decrease in all the A values, (ii) no change in the B constants for the D levels, and (iii) a decrease in this B constant for the P levels for the CC SD $nl \in \{5p,5s,4p,4s\}$ RCI calculations, for both optimization strategies. However, the agreement with experimental values is not as good as in ^{137}Ba II or ^{87}Sr II, the best being a 0.2% difference for the $A(^3D_2)$ constant, and the worst being 80% for the $A(^1D_2)$ constant. Note that there exists a systematic trend where the largest discrepancy with experiment is often obtained for the smaller HFS constants, such as the $A(^2D_{5/2})$ constant in ^{137}Ba II.

Table 8. Magnetic dipole A and electric quadrupole B hyperfine structure constants (in MHz) of ^{137}Ba I obtained for AS7 ($I = 3/2, \mu = 0.9375\mu_N, Q = 0.236$ b [34]), compared to available theoretical and experimental data. The recommended values are given in the form of $\mu \pm 2\sigma$, exhibiting a 95% confidence level. *: Number of CSFs obtained after reduction using the rcsfginteract_csfg code; [a]: Th. Olsson et al. (DF, MCDF) [16]; [b]: Th. Tang (RCC) [53]; [c]: Th. Kozlov et al. (RMBPT) [54]; [d]: Expt. Gustavsson et al. [56]; [e]: Expt. Schmelling [55]; [f]: Expt. Kluge et al. [57]; [g]: Expt. zu Putlitz [58].

Strategy	$^3D_1$			$^1D_2$			$^3D_2$			$^1P_1^o$		$^3P_1^o$	
	N_{CSFs}	A	B	N_{CSFs}	A	B	A	B	N_{CSFs}	A	B	A	B
Single reference													
MCDHF VV SrD	557	−353	12	815	−22	38	301	17	194	−45	25	787	−25
RCI CC SD $nl \geq 5s$	27,750 *	−434	9	94,033 *	−10	33	251	13	46,739 *	−30	33	851	−27
RCI CC SD $nl \in \{5p, 5s, 4p, 4s\}$	54,943 *	−446	11	187,251 *	−5	40	256	17	92,909 *	−24	36	872	−28
MCDHF VVSrD + CV SrD $nl \geq 5s$	37,522	−513	11	53 330	−77	37	400	16	28,368	−95	35	1084	−37
RCI CC SD $nl \geq 5s$	48,471 *	−500	12	140,798 *	−23	39	328	17	73,025 *	−60	32	967	−29
RCI CC SD $nl \in \{5p, 5s, 4p, 4s\}$	96,385 *	−524	15	280,781 *	−19	48	338	22	103,635 *	−60	32	967	−29
MCDHF VV SrD + CV SrD $nl \geq 4p$	55,291 *	−546	18	129,863 *	−79	56	456	28	77,458	−102	43	1216	−42
RCI CC SD $nl \geq 5s$	84,190 *	−526	18	226,898 *	−21	57	372	27	119,259 *	−69	37	1067	−33
RCI CC SD $nl \in \{5p, 5s, 4p, 4s\}$	117,852 *	−547	18	334,107 *	−17	56	371	26	173,007 *	−64	37	1073	−32
Multireference													
MCDHF VV SrD	557	−353	12	815	−22	38	301	17	614	−46	26	788	−25
RCI CC SD $nl \geq 5s$	75,823 *	−479	10	235,817 *	−40	32	290	14	165,636 *	−86	30	898	−23
RCI CC SD $nl \in \{5p, 5s, 4p, 4s\}$	151,089 *	−491	12	470,819 *	−40	38	296	17	330,658 *	−88	31	908	−23
MCDHF VV SrD + CV SrD $nl \geq 5s$	36,420 *	−513	11	52,895 *	−80	36	402	16	60,610 *	−119	33	947	−24
RCI CC SD $nl \geq 5s$	110,102 *	−517	10	285,738 *	−67	32	362	16	222,175 *	−41	34	866	−23
RCI CC SD $nl \in \{5p, 5s, 4p, 4s\}$	185,368 *	−532	13	520,740 *	−67	38	368	19	387,197 *	−38	34	862	−23
MCDHF VV SrD + CV SrD $nl \geq 4p$	101,890 *	−545	18	148,083 *	−88	54	465	27	164,291 *	−108	32	925	−21
RCI CC SD $nl \geq 5s$	175,572 *	−546	17	380,926 *	−74	48	414	24	327,304 *	−101	26	877	−18
RCI CC SD $nl \in \{5p, 5s, 4p, 4s\}$	249,704 *	−564	16	614,395 *	−75	46	415	24	490,884 *	−103	26	875	−18
This work, recommended		-517 ± 85	14 ± 5		-37 ± 57	44 ± 14	341 ± 115	21 ± 8		-63 ± 59	33 ± 8	926 ± 163	-26 ± 10
Th. [a]		−368	19		−13	41	320	48		−53	−8	804	53
Th. [b]		-514 ± 14			-84 ± 4		421 ± 11			-112 ± 2			
Th. [c]		−547	18		−102	67	405	27		−107	51	1160	−43
Expt.		-520.536 ± 0.003 [d]	17.890 ± 0.003 [d]		-82.180 ± 0.003 [e]	59.564 ± 0.014 [e]	415.928 ± 0.003 [d]	25.899 ± 0.013 [d]		-109.2 ± 1.2 [f]	51 ± 12 [f]	1150.59 ± 0.02 [g]	-41.61 ± 0.02 [g]

Enlarging the reference set (SR → MR) yields better results for the largest MCDHF calculations based on the VV SrD + CV SrD $nl \geq 4p$ + RCI CC SD $nl \in \{5p, 5s, 4p, 4s\}$ strategy, especially for the $A(^1D_2)$ and $A(^1P_1^o)$ hyperfine constants for which the two-configuration mixing found in the MR wave functions are particularly large. The $A(^1D_2)$ value decreases from −17 to −75 MHz, in much better agreement (≃10%) with observation. The use of a MR also reduces drastically the $A(^1P_1^o)$ value, from −64.06 MHz to −103.07 MHz, achieving a 6% agreement with experiments. However, the B constants are also decreased by ≈10 MHz, deteriorating the agreement with experimental values.

The theory–experiment agreement is the best for the MR calculations in the D levels, but is still acceptable in the recommended values. This work gives the best MCDHF values as well as an uncertainty determination, uncommon for such works. This was achieved by taking into account deeper core correlations, when they were totally neglected in the Olsson et al. study [16], and therefore missed the crucial CV correlations, essential for an accurate description of the HFS. Moreover, the 2σ uncertainty covers most of the experimental results.

The transformation into natural orbitals has also been studied. In the case of the SR, the impact on the D levels is limited. The B hyperfine constants do not significantly change using the NOs, with the highest change of +0.2 MHz for the $^1D_2$ level. However, the effect on the A constants is a bit larger, improving the agreement with experiment for the $^3D_{1,2}$ levels, but degrading it for the $^1D_2$ level. The improvement is similar for the odd levels. Applying the natural orbitals in the MR case does not significantly improve the theory–observation agreement for all levels. Therefore, the applicability of the developed MCDHF CV SrD $nl \geq 4p$ + RCI CC SD $nl \in \{5p, 5s, 4p, 4s\}$ strategy in ^{137}Ba II is not as straightforward as in ^{87}Sr II.

4. Conclusions

This work has enabled an in-depth study of the hyperfine structure of the astrophysically relevant atomic levels of ^{137}Ba I, ^{135,137}Ba II, and ^{87}Sr II, using relativistic atomic calculations based on the MCDHF/RCI method as implemented in the GRASP package. The main objective was to estimate hyperfine structure constants, within a unified model for selected levels and for elements with similar atomic structures, in order to improve the interpretation of stellar spectra.

The detailed analysis of ^{137}Ba II revealed that each level requires a tailored optimization strategy. For instance, the A hyperfine constant is optimally described by focusing on core–valence (CV) correlations limited to $nl \geq 5s$, while the B constant needs deeper correlations extending to $4p$ electrons. This distinction underscores the different sensitivity of A and B to electron correlation effects, confirmed by the statistical spread of recommended values. The persistent discrepancy of the $A(^2D_{5/2})$ constant highlights the challenges in determining accurate small HFS constants in heavy elements. While the inclusion of higher-order correlations (triple substitutions) improved both A and B constants for the odd levels, the $A(^2D_{5/2})$ issue remains unresolved.

The MCDHF model developed for ^{137}Ba II was directly applicable to ^{87}Sr II, yielding results in very good agreement with the experiment. The smallest HFS constant, $A(^2D_{5/2})$, was found to be highly sensitive to the orbital basis, reflecting internal cancellations between orbital, spin-dipolar, and Fermi contact terms in the non-relativistic framework. This work provides the first theoretical uncertainty estimates for levels lacking experimental data (e.g., $^2D_{3/2}$ and $^2P_{1/2}^o$), which are critical for astrophysical applications.

Finally, the complexity of ^{137}Ba I, arising from its two valence electrons, necessitated a multireference approach to account for non-negligible configuration mixing. While MR calculations significantly improved the $A(^1D_2)$ and $A(^1P_1^o)$ constants, achieving less than

10% discrepancy with experiment, the theory–observation gap remains larger than for ^{135,137}Ba II or ^{87}Sr II. Nevertheless, this study enables theoretical uncertainty quantification and represents the most accurate MCDHF calculations for HFS constants since the work of Olsson et al. [16].

Our recommended values enable a qualitative connection to the determination of $f_{\mathrm{odd,Ba}}$. If the hyperfine structure (HFS) constants are systematically overestimated, the resulting spectral lines exhibit greater broadening and asymmetry than observed experimentally. To align the modeled spectra with observations, the isotopic ratio $f_{\mathrm{odd,Ba}}$ must be adjusted downward, with the effect of reducing the contribution of odd isotopes. On the other hand, underestimation of the HFS constants would necessitate an upward adjustment of $f_{\mathrm{odd,Ba}}$, amplifying the odd isotope abundances in the modeled spectra. This adjustment could ultimately lead to incorrect conclusions about the nucleosynthesis process.

This study tested new code developments for improving hyperfine structure calculations in heavy elements. Polarization orbitals, integrated into the orbital basis via energy-functional optimization that showed promise for light elements (e.g., Li [38] and N [29]), were partially tested due to the high computational load in ^{137}Ba II. The reduction in the number of required CSFs could enable deeper electron correlation studies without sacrificing accuracy. The upcoming integration of Partitioned Correlation Functions (PCFs) [59] into GRASPG [60] is expected to significantly reduce computational demands, enabling more efficient calculations. Natural orbitals were also explored to refine hyperfine constants by relaxing core–valence polarization and improving near-nuclear electron density. For ^{135,137}Ba II and ^{87}Sr II, natural orbitals systematically adjusted A and B constants (increasing positive values and decreasing negative ones), consistent with prior observations in Na [43]. However, their impact on ^{137}Ba I was negligible.

Future studies should incorporate isotope shifts (IS), currently neglected due to their small magnitude, to achieve a holistic modeling of stellar line profiles. A combined HFS + IS analysis would further refine $f_{\mathrm{odd,Ba}}$ determinations and enhance the reliability of galactic chemical evolution models.

Author Contributions: Conceptualization, L.N., L.M. and P.P.; methodology, L.N., L.M., P.P. and P.J.; software, P.J.; validation, L.N., L.M., P.P., P.J. and M.G.; formal analysis, L.N.; investigation, L.N.; resources, L.N., L.M. and P.P.; data curation, L.N., L.M. and P.P.; writing—original draft preparation, L.N., L.M. and P.P.; writing—review and editing, L.N., L.M., P.P., P.J. and M.G.; visualization, P.P.; supervision, L.M. and P.P.; project administration, P.P.; funding acquisition, P.P. All authors have read and agreed to the published version of the manuscript.

Funding: This research was funded by F.R.S.-FNRS–EOS grant number O.0004.22. This project received funding from the FWO and F.R.S.-FNRS under the Excellence of Science (EOS) program (number O.0004.22). Part of the atomic calculations were made with computational resources provided by the Consortium des Equipements de Calcul Intensif (CECI), funded by the F.R.S.-FNRS under grant no. 2.5020.11 and by the Walloon Region of Belgium. P.J. acknowledges support from the Swedish Research Council (VR 2023-05367).

Data Availability Statement: The original contributions presented in this study are included in the article.

Acknowledgments: P.P. is Research Associate of the Belgian Fund for Scientific Research F.R.S.-FNRS.

Conflicts of Interest: The authors declare no conflicts of interest. The funders had no role in the design of the study; in the collection, analyses, or interpretation of data; in the writing of the manuscript; or in the decision to publish the results.

Abbreviations

The following abbreviations are used in this manuscript:

3D-LTE	3D Local Thermodynamic Equilibrium
AMPSCI	Atomic Many-body Perturbation theory in the Screened Coulomb Interaction
AS	Active Set
ASF	Atomic State Function
CC	Core–Core
CEMP	Carbon-Enhanced Metal-Poor
CSF	Configuration State Function
CSFG	Configuration State Function Generator
CV	Core–Valence
D	Double
DHF	Dirac–Hartree–Fock
GRASP	General Relativistic Atomic Structure Package
HF	Hartree–Fock
HFS	Hyperfine Structure
IS	Isotope Shift
MCDHF	Multiconfiguration Dirac–Hartree–Fock
MCHF	Multiconfiguration Hartree–Fock
MR	MultiReference
NO	Natural Orbital
PCF	Partitioned Correlation Function
RCC	Relativistic Coupled Cluster
RCI	Relativistic Configuration Interaction
RMBPT	Relativistic Many-Body Perturbation Theory
S	Single
SrD	Single and restricted Double
SR	Single Reference
VV	Valence–Valence

References

1. Busso, M.; Gallino, R.; Wasserburg, G.J. Nucleosynthesis in Asymptotic Giant Branch Stars: Relevance for Galactic Enrichment and Solar System Formation. *Annu. Rev. Astron. Astrophys.* **1999**, *37*, 239–309. [CrossRef]
2. Lugaro, M.; Pignatari, M.; Reifarth, R.; Wiescher, M. The s-Process and Beyond. *Annu. Rev. Nucl. Part. Sci.* **2023**, *73*, 315–340. [CrossRef]
3. Cowan, J.J.; Rose, W.K. Production of C-14 and neutrons in red giants. *Astrophys. J.* **1977**, *212*, 149. [CrossRef]
4. Arlandini, C.; Kappeler, F.; Wisshak, K.; Gallino, R.; Lugaro, M.; Busso, M.; Straniero, O. Neutron Capture in Low-Mass Asymptotic Giant Branch Stars: Cross Sections and Abundance Signatures. *Astrophys. J.* **1999**, *525*, 886–900. [CrossRef]
5. Peterson, R.C. The Extreme Overabundance of Molybdenum in two Metal-Poor Stars. *Astrophys. J.* **2011**, *742*, 21. [CrossRef]
6. Lambert, D.L.; Allende Prieto, C. The isotopic mixture of barium in the metal-poor subgiant HD 140283. *Mon. Not. R. Astron. Soc.* **2002**, *335*, 325–334. [CrossRef]
7. Gallagher, A.J.; Ludwig, H.G.; Ryan, S.G.; Aoki, W. A three-dimensional hydrodynamical line profile analysis of iron lines and barium isotopes in HD 40283. *Astron. Astrophys.* **2015**, *579*, A94. [CrossRef]
8. Reddy, A.B.S.; Lambert, D.L. Local associations and the barium puzzle. *Mon. Not. R. Astron. Soc.* **2015**, *454*, 1976–1991. [CrossRef]
9. Hansen, C.J.; Bergemann, M.; Cescutti, G.; François, P.; Arcones, A.; Karakas, A.I.; Lind, K.; Chiappini, C. LTE or non-LTE, that is the question: The NLTE chemical evolution of strontium in extremely metal-poor stars. *Astron. Astrophys.* **2013**, *551*, A57. [CrossRef]
10. Barbuy, B.; Cayrel, R.; Spite, M.; Beers, T.C.; Spite, F.; Nordström, B.; Nissen, P.E. Analysis of two CH/CN-strong very metal-poor stars. *Astron. Astrophys.* **1997**, *317*, L63–L66.
11. Van Eck, S.; Giribaldi, R.; Merle, T.; Lambotte, A.; Karinkuzhi, D.; Goriely, S.; Choplin, A.; Storm, N.; Gerber, J.; Siess, L.; et al. From the s-Process to the i-Process: A New Perspective on the Chemical Enrichment of Extrinsic Stars. *Galaxies* **2024**, *12*, 89. [CrossRef]
12. Magain, P.; Zhao, G. Barium isotopes in the very metal-poor star HD 140283. *Astron. Astrophys.* **1993**, *268*, L27–L29.

13. Grant, I.P. *Relativistic Quantum Theory of Atoms and Molecules*; Springer: New York, NY, USA, 2007. [CrossRef]
14. Froese Fischer, C.; Gaigalas, G.; Jönsson, P.; Bieroń, J. GRASP—2018—A Fortran 95 version of the General Relativistic Atomic Structure Package. *Comput. Phys. Commun.* **2019**, *237*, 184–187. [CrossRef]
15. Itano, W. Quadrupole moments and hyperfine constants of metastable states of Ca^+, Sr^+, Ba^+, Yb^+, Hg^+ and Au. *Phys. Rev. A* **2006**, *73*, 022510. [CrossRef]
16. Olsson, T.; Rosén, A.; Fricke, B.; Torbohm, G. Analysis of the electronic structure, hyperfine structure, and volume isotope shifts in the low lying states of Ba I and Ba II. *Phys. Scr.* **1988**, *37*, 730–741. [CrossRef]
17. Lindgren, I.; Morrison, J. *Atomic Many-Body Theory*; Springer: Berlin/Heidelberg, Germany, 1986. [CrossRef]
18. Jönsson, P.; Godefroid, M.; Gaigalas, G.; Ekman, J.; Grumer, J.; Li, W.; Li, J.; Brage, T.; Grant, I.P.; Bieroń, J.; et al. An Introduction to Relativistic Theory as Implemented in GRASP. *Atoms* **2022**, *11*, 7. [CrossRef]
19. Dyall, K.; Grant, I.; Johnson, C.; Parpia, F.; Plummer, E. GRASP: A general-purpose relativistic atomic structure program. *Comput. Phys. Commun.* **1989**, *55*, 425–456. [CrossRef]
20. Jönsson, P.; Gaigalas, G.; Fischer, C.F.; Bieroń, J.; Grant, I.P.; Brage, T.; Ekman, J.; Godefroid, M.; Grumer, J.; Li, J.; et al. GRASP Manual for Users. *Atoms* **2023**, *11*, 68. [CrossRef]
21. Si, R.; Li, Y.; Wang, K.; Chen, C.; Gaigalas, G.; Godefroid, M.; Jönsson, P. GRASPG—An extension to GRASP2018 based on configuration state function generators. *Comput. Phys. Commun.* **2025**, *312*, 109604. [CrossRef]
22. Papoulia, A.; Schiffmann, S.; Bieroń, J.; Gaigalas, G.; Godefroid, M.; Harman, Z.; Jönsson, P.; Oreshkina, N.S.; Pyykkö, P.; Tupitsyn, I.I. Ab initio electronic factors of the A and B hyperfine structure constants for the $5s^25p6s\ ^{1,3}P^o_1$ states in Sn I. *Phys. Rev. A* **2021**, *103*, 022815. [CrossRef]
23. Sahoo, B.K.; Das, B.P.; Chaudhuri, R.K.; Mukherjee, D. Theoretical studies of the $6s\ ^2S_{1/2} \rightarrow 5d\ ^2D_{3/2}$ parity-nonconserving transition amplitude in Ba^+ and associated properties. *Phys. Rev. A* **2007**, *75*, 032507. [CrossRef]
24. Safronova, U.I. Relativistic many-body calculation of energies, lifetimes, hyperfine constants, multipole polarizabilities, and blackbody radiation shift in ^{137}Ba II. *Phys. Rev. A* **2010**, *81*, 052506. [CrossRef]
25. Blatt, R.; Werth, G. Precision determination of the ground-state hyperfine splitting in $^{137}Ba^+$ using the ion-storage technique. *Phys. Rev. A* **1982**, *25*, 1476–1482. [CrossRef]
26. Silverans, R.E.; Borghs, G.; De Bisschop, P.; Van Hove, M. Hyperfine structure of the $5d\ ^2D_J$ states in the alkaline-earth Ba ion by fast-ion-beam laser-rf spectroscopy. *Phys. Rev. A* **1986**, *33*, 2117–2120. [CrossRef]
27. Villemoes, P.; Arnesen, A.; Heijkenskjold, F.; Wannstrom, A. Isotope shifts and hyperfine structure of $^{134-138}$Ba II by fast ion beam-laser spectroscopy. *J. Phys. B* **1993**, *26*, 4289–4299. [CrossRef]
28. Wendt, K.; Ahmad, S.A.; Buchinger, F.; Mueller, A.C.; Neugart, R.; Otten, E.W. Relativistic J-dependence of the isotope shift in the $6s - 6p$ doublet of Ba II. *Z. Phys. A* **1984**, *318*, 125–129. [CrossRef]
29. Ma, M.; Li, Y.; Godefroid, M.; Gaigalas, G.; Li, J.; Bieroń, J.; Chen, C.; Wang, J.; Jönsson, P. Natural Orbitals and Targeted Non-Orthogonal Orbital Sets for Atomic Hyperfine Structure Multiconfiguration Calculations. *Atoms* **2024**, *12*, 30. [CrossRef]
30. Bieroń, J.; Froese Fischer, C.; Indelicato, P.; Jönsson, P.; Pyykkö, P. Complete-active-space multiconfiguration Dirac-Hartree-Fock calculations of hyperfine-structure constants of the gold atom. *Phys. Rev. A* **2009**, *79*, 052502. [CrossRef]
31. Fischer, C.F.; Brage, T.; Jönsson, P. *Computational Atomic Structure: An MCHF Approach*; Routledge: London, UK, 1997. [CrossRef]
32. Bieroń, J.; Filippin, L.; Gaigalas, G.; Godefroid, M.; Jönsson, P.; Pyykkö, P. Ab initio calculations of the hyperfine structure of zinc and evaluation of the nuclear quadrupole moment $Q(^{67}\mathrm{Zn})$. *Phys. Rev. A* **2018**, *97*, 062505. [CrossRef]
33. Yuan, X.; Panigrahy, S.N.; Dougherty, R.W.; Das, T.P.; Andriessen, J. Hyperfine strucutres of Ca^+ and Sr^+ ions: Summary of trends in hyperfine interactions in the alkaline-earth metal ions and corresponding series with similar electronic structures. *Phys. Rev. A* **1995**, *52*, 197–207. [CrossRef] [PubMed]
34. Mertzimekis, T.J.; Stamou, K.; Psaltis, A. An online database of nuclear electromagnetic moments. *Nucl. Instruments Methods Phys. Res. Sect. A Accel. Spectrometers Detect. Assoc. Equip.* **2016**, *807*, 56–60. [CrossRef]
35. Safronova, U.I. All–order perturbation calculation of energies, hyperfine constants, multipole polarizabilities, and blackbody radiation shift in ^{87}Sr II. *Phys. Rev. A* **2010**, *82*, 022504. [CrossRef]
36. Engels, B. Study of influences of various excitation classes on ab initio calculated isotropic hyperfine coupling constants. *Theor. Chem. Acc.* **1993**, *86*, 429–437. [CrossRef]
37. Bieroń, J.; Fischer, C.F.; Fritzsche, S.; Gaigalas, G.; Grant, I.P.; Indelicato, P.; Jönsson, P.; Pyykkö, P. Ab initio MCDHF calculations of electron–nucleus interactions. *Phys. Scr.* **2015**, *90*, 054011. [CrossRef]
38. Li, Y.; Jönsson, P.; Godefroid, M.; Gaigalas, G.; Bieroń, J.; Marques, J.P.; Indelicato, P.; Chen, C. Independently Optimized Orbital Sets in GRASP—The Case of Hyperfine Structure in Li I. *Atoms* **2022**, *11*, 4. [CrossRef]
39. Werner, H. Matrix-Formulated Direct Multiconfiguration Self-Consistent Field and Multiconfiguration Reference Configuration-Interaction Methods. In *Advances in Chemical Physics*; Wiley Online Library: Hoboken, NJ, USA, 1987; pp. 1–62. [CrossRef]
40. Knowles, P.; Schütz, M.; Werner, H.J. *Modern Methods and Algorithms of Quantum Chemistry, Proceedings*; NIC Series; John von Neumann Institute for Computing: Jülich, Germany, 2000; pp. 97–179.

41. Lindgren, I.; Lindgren, J.; Mårtensson, A.M. Many-body calculations of the hyperfine interaction of some excited states of alkali atoms, using approximate Brueckner or natural orbitals. *Z. Phys. A* **1976**, *279*, 113–125. [CrossRef]
42. Schiffmann, S.; Li, J.; Ekman, J.; Gaigalas, G.; Godefroid, M.; Jönsson, P.; Bieroń, J. Relativistic radial electron density functions and natural orbitals from GRASP2018. *Comput. Phys. Commun.* **2022**, *278*, 108403. [CrossRef]
43. Schiffmann, S.; Godefroid, M.; Ekman, J.; Jönsson, P.; Fischer, C.F. Natural orbitals in multiconfiguration calculations of hyperfine-structure parameters. *Phys. Rev. A* **2020**, *101*, 062510. [CrossRef]
44. Lu, B.; Lu, X.; Wang, T.; Chang, H. Ab initio calculations of the hyperfine structure of ^{109}Cd, ^{109}Cd^{+} and reevaluation of the nuclear quadrupole moment $Q(^{109}\mathrm{Cd})$. *J. Phys. B* **2022**, *55*, 205002. [CrossRef]
45. Martensson-Pendrill, A.M.; Ynnerman, A. Isotope shift and nuclear charge radii of barium isotopes. *J. Phys. B* **1992**, *25*, L551–L559. [CrossRef]
46. Sahoo, B.K.; Barrett, M.D.; Das, B.P. Reliability test for the experimental results of electric-quadrupole hyperfine-structure constants and assessment of nuclear quadrupole moments in ^{135}Ba and ^{137}Ba. *Phys. Rev. A* **2013**, *87*, 042506. [CrossRef]
47. Cserveny, R.B.; Roberts, B.M. Theoretical characterization of the barium II and radium II ions. *Phys. Rev. A* **2025**, *112*, 032816. [CrossRef]
48. Sunaoshi, H.; Fukashiro, Y.; Furukawa, M.; Yamauchi, M.; Hayashibe, S.; Shinozuka, T.; Fujioka, M.; Satoh, I.; Wada, M.; Matsuki, S. A precision measurement of the hyperfine structure of ^{87}Sr^{+}. *Hyperfine Interact.* **1993**, *78*, 241–245. [CrossRef]
49. Barwood, G.P.; Gao, K.; Gill, P.; Huang, G.; Klein, H.A. Observation of the hyperfine structure of the $^{2}S_{1/2} - {}^{2}D_{5/2}$ transition in ^{87}Sr^{+}. *Phys. Rev. A* **2003**, *67*, 013402. [CrossRef]
50. Buchinger, F.; Ramsay, E.B.; Arnold, E.; Neu, W.; Neugart, R.; Wendt, K.; Silverans, R.E.; Lievens, P.; Vermeeren, L.; Berdichevsky, D.; et al. Systematics of nuclear ground state properties in $^{78-100}$Sr by laser spectroscopy. *Phys. Rev. C* **1990**, *41*, 2883–2897. [CrossRef]
51. Boualili, F.Z.; Nemouchi, M.; Godefroid, M.; Jönsson, P. Weak correlation and strong relativistic effects on the hyperfine interaction in fluorine. *Phys. Rev. A* **2021**, *104*, 062813. [CrossRef]
52. Sahoo, B.K.; Jönsson, P.; Gaigalas, G. Comparative analysis of Mg^{+} properties using multiconfiguration Dirac-Hartree-Fock and relativistic coupled-cluster methods. *Phys. Rev. A* **2025**, *112*, 012809. [CrossRef]
53. Tang, Y.B. Determination of nuclear quadrupole moments for ^{25}Mg, ^{87}Sr, and ^{135,137}Ba via configuration-interaction combined with a coupled-cluster approach. *arXiv* **2025**, arXiv:2512.07603v2. [CrossRef]
54. Kozlov, M.; Porsev, S. Polarizabilities and hyperfine structure constants of the low-lying levels of barium. *Eur. Phys. J. D* **1999**, *5*, 59–63. [CrossRef]
55. Schmelling, S.G. Hyperfine structure in the metastable *D* states of atomic barium. *Phys. Rev. A* **1974**, *9*, 1097–1102. [CrossRef]
56. Gustavsson, M.; Olsson, G.; Rosén, A. Hyperfine-structure investigation in the 6*s*5*d* configuration of ^{135}Ba and ^{137}Ba. *Z. Phys. A* **1979**, *290*, 231–243. [CrossRef]
57. Kluge, H.J.; Sauter, H. Levelcrossing experiments in the first excited $^{1}P_{1}$ states of the alkaline earths. *Z. Phys.* **1974**, *270*, 295–309. [CrossRef]
58. Zu Putlitz, G. Bestimmung der elektrischen Kernquadrupolmomente der beiden ungeraden stabilen Bariumisotope ^{135}Ba und ^{137}Ba. *Ann. Phys.* **1963**, *466*, 248–260. [CrossRef]
59. Verdebout, S.; Rynkun, P.; Jönsson, P.; Gaigalas, G.; Fischer, C.F.; Godefroid, M. A partitioned correlation function interaction approach for describing electron correlation in atoms. *J. Phys. B* **2013**, *46*, 085003. [CrossRef]
60. Wu, S.; Si, R.; Chen, C.; Gaigalas, G.; Godefroid, M.; Jönsson, P. Private communication, in preparation, 2026.